Light-induced current in molecular junctions: Local field and non-Markov effects

Boris D. Fainberg,[1] Maxim Sukharev,[2] Tae-Ho Park,[3] and Michael Galperin[3]
[1]*Faculty of Sciences, Holon Institute of Technology, Holon 58102, Israel*
[2]*Department of Applied Sciences and Mathematics, Arizona State University at the Polytechnic Campus, Mesa, Arizona 85212, USA*
[3]*Department of Chemistry & Biochemistry, University of California at San Diego, La Jolla, California 92093, USA*
(Received 9 March 2011; revised manuscript received 11 April 2011; published 23 May 2011)

We consider a two-level system coupled to contacts as a model for a charge pump under external laser pulse. The model represents a charge-transfer molecule in a junction and is a generalization of previously published results [B. D. Fainberg, M. Jouravlev, and A. Nitzan, Phys. Rev. B **76**, 245329 (2007)]. Effects of local field for realistic junction geometries and non-Markov response of the molecule are taken into account within finite-difference time-domain and on-the-contour equation-of-motion formulations, respectively. We find that contrary to the symmetric behavior of the pump relative to the chirp sign, the duration of the corresponding local-field pulse does depend on the chirp sign, which results in an asymmetric charge pumping. The most effective charge-pump regime is found at positive bias, contrary to Markov consideration of the previous study.

DOI: 10.1103/PhysRevB.83.205425 PACS number(s): 73.23.−b, 78.20.Jq, 78.67.−n, 85.60.−q

I. INTRODUCTION

Driven transport and coherent control at the nanoscale are well-established areas of research. Quantum ratchets,[1,2] molecular charge,[3] spin[4,5] and heat pumps,[6,7] and nanoplasmonics[8] are just several examples of areas of recent development. Advances in optical techniques, in particular near-field optical microscopy, allow single-molecule manipulation[9] and induction of bond-specific chemistry.[10] Combined with molecular junction fabrication techniques,[11] optical spectroscopy methods are becoming an important observation and diagnostic tool in molecular electronics.[12–14]

Experimental developments led to a surge of theoretical activity in the field of optically assisted transport[15–18] and optical response of molecular junctions.[19–25]

In particular, Ref. 16 considered molecular junctions composed of molecules with a strong charge-transfer transition into their excited state[26–28] as a possible constituent for light-induced molecular charge pump when change of molecular dipole occurs along the junction axis. The consideration was done within a two-level (HOMO-LUMO) model with the ground (HOMO) and excited (LUMO) states of the molecule strongly coupled to different contacts. In the junction setup, optical excitations bring electrons from occupied ground to empty excited states and the asymmetry in coupling to contacts assures appearance of a current. The model was treated within the nonequilibrium Green function approach, and the perturbation theory was employed in relation to the laser field coupling.

Later, Ref. 29 generalized the consideration of Ref. 16 to strong laser fields. The pumping optical field was treated as a classical driving force and a closed set of equations of motion (EOM) for observables (i.e., electronic populations and coherences of the levels, and single-time exciton correlation function) was formulated. One of the most important advances in Ref. 29 was a consideration of chirped laser pulses, which allowed for a formulation of the charge-transfer process between ground and excited states in terms of the Landau-Zener problem. Chirped laser pulses enable to produce a complete population inversion in molecular systems (such as a molecular bridge) where the well-known π-pulse excitation[30] fails.

In realistic molecular junctions, the optical field driving the molecule is a *local field* formed by both the incident radiation and the scattered response of the system (mostly plasmonic response of metallic contacts). Another feature of molecular junctions is the hybridization of states of a molecule with those of contacts. The latter leads to non-Markov effects in the response of the junction.

In this paper we generalize the studies reported in Ref. 29 by incorporating the aforementioned effects into our consideration. The dynamics of local electromagnetic fields is simulated within the finite-difference time-domain (FDTD) technique for a realistic geometry of a molecular junction, similar to our previous publication.[23] Non-Markov effects of the junction response are introduced within a nonequilibrium-Green-function equation-of-motion (NEGF-EOM) approach.

The structure of the paper is the following. After introducing the model in Sec. II, we describe the junction geometry and the numerical approach used in our calculations of local electromagnetic fields in Sec. III. Section IV discusses our calculations of the local-field-induced electron flux through the junction, and Sec. V introduces a set of NEGF equations of motion. The numerical results and related discussion are given in Sec. VI. Section VII summarizes our findings.

II. MODEL

A model junction consists of a molecule coupled to two metallic contacts driven by an external radiation field. The radiation is a time-dependent local electromagnetic field, $E(t)$, calculated within the FDTD technique for bowtie geometry of the contacts (see Sec. III for details). The molecule is represented by a two-level system, $|1\rangle$ and $|2\rangle$ (HOMO and LUMO or ground and excited states), and is placed in a "hot spot" of the local field. The contacts L and R are assumed to be free-charge-carrier reservoirs, each at its own equilibrium. The difference in their electrochemical potentials defines the bias applied to the junction, $eV = \mu_L - \mu_R$. Following Refs. 16 and 29, we consider two types of coupling between the molecule and the contacts: charge and energy transfer. The

Hamiltonian of the junction is

$$\hat{H}(t) = \hat{H}_0(t) + \hat{V}, \tag{1}$$

$$\hat{H}_0(t) = \sum_{m=1,2} \varepsilon_m \hat{n}_m + \sum_{k\in\{L,R\}} \varepsilon_k \hat{n}_k - \mu E(t)(\hat{D}_{12} + \hat{D}_{12}^\dagger), \tag{2}$$

$$\hat{V} = \sum_{m=1,2} \sum_{k\in\{L,R\}} (V_{km} \hat{c}_k^\dagger \hat{d}_m + \text{H.c.}) + \sum_{k_1\neq k_2\in\{L,R\}} \left(V_{k_1k_2}^{\text{en}} \hat{c}_{k_1}^\dagger \hat{c}_{k_2} \hat{D}_{12} + \text{H.c.}\right), \tag{3}$$

Here, $\hat{d}_m^\dagger$ ($\hat{d}_m$) and $\hat{c}_k^\dagger$ ($\hat{c}_k$) are creation (annihilation) operators of an electron in a level m of the molecule and in a state k in the contact(s), respectively. $\hat{n}_m = \hat{d}_m^\dagger \hat{d}_m$ is the operator of electronic population in a level m, $\hat{D}_{12} \equiv \hat{d}_1^\dagger \hat{d}_2$ is the operator of molecular de-excitation ($\hat{D}_{21} \equiv \hat{D}_{12}^\dagger$), and μ is the molecular transition dipole moment. The terms on the right-hand side of Eq. (2) represent the molecular structure (a two-level system), the contacts, and the coupling to the driving field. The right-hand side of Eq. (3) introduces electron and energy transfer between the molecule and the contact(s). Here, V_{km} is the matrix element of electron tunneling from a molecular level m into a state k in the contact and $V_{k_1k_2}^{\text{en}}$ is the matrix element of exciton transfer from the molecule to the contact(s). The latter is caused by the dipolar interaction between molecular excitation and electron-hole pairs in the metal.

Eqs. (1)–(3) introduce the model of Ref. 29, but with the rotating-wave approximation relaxed and with the driving force treated as a local electromagnetic field.

To simulate molecules with strong charge-transfer transitions with the dipole moment oriented along the junction axis, below we assume that the ground state (or HOMO), $|1\rangle$, is coupled strongly to the left contact, L, while the excited state (or LUMO) is strongly coupled to the right contact, R. Such setup works as a local-field-driven charge pump (see Fig. 1). Note that a similar selective coupling can also be obtained for a bridge made of quantum dots as discussed in Refs. 31–33.

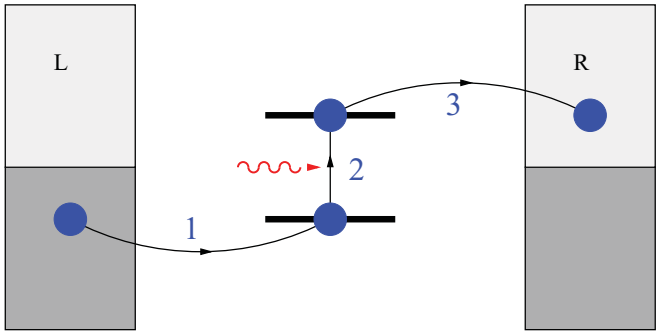

FIG. 1. (Color online) A sketch of local field-driven-molecular-charge pump.

III. LOCAL FIELD SIMULATIONS

Calculations of the local-electromagnetic-field dynamics are carried out utilizing the FDTD technique.[34] Following Ref. 29 we assume that the incident field, $E_{\text{inc}}(t)$, has the form of a linear chirped pulse

$$E_{\text{inc}}(t) = \text{Re}\left[\mathcal{E}_0 \exp\left(-\frac{(\delta^2 - i\bar{\mu})t^2}{2} - i\omega_0 t\right)\right], \tag{4}$$

where $\mathcal{E}_0$ is the incident peak amplitude, ω_0 is the incident frequency, and the parameters δ and $\bar{\mu}$ describing an incident chirped pulse are given by

$$\delta^2 = \frac{2\tau_0^2}{\tau_0^4 + 4\Phi''^2(\omega_0)}, \tag{5}$$

$$\bar{\mu} = -\frac{4\Phi''(\omega_0)}{\tau_0^4 + 4\Phi''^2(\omega_0)}, \tag{6}$$

with $\tau_0 \equiv t_{p0}/\sqrt{2\log 2}$ (the value of the pulse duration, t_{p0}, of the corresponding transform-limited pulse used in our simulations is 9.34 fs) and $\Phi''(\omega_0)$ is the chirp rate in the frequency domain. Throughout the simulations the incident field is taken in the form of Eq. (4) and is normalized to preserve the total energy of a laser pulse at different chirp rates according to

$$\int_{-\infty}^{+\infty} dt\, E_{\text{inc}}^2(t) = \text{const}. \tag{7}$$

The geometry considered is depicted in the inset of Fig. 2(a) showing the top view of the bowtie antenna. To investigate the influence of chirped incident pulses on plasmon dynamics we choose an incident field in the form of Eq. (4) and vary $\Phi''(\nu_0) = 4\pi^2\Phi''(\omega_0)$. Below we shall write Φ'' having in mind $\Phi''(\nu_0)$. We further presume that the incident pulse is x-polarized and propagates along the z axis with the incident frequency at the plasmon resonance [see the inset of Fig. 2(a)]. The material dispersion of silver is taken in the Drude form with other numerical parameters as in Ref. 23. For a given set of material and geometric parameters, the local-electric-field enhancement exhibits a well-pronounced plasmon resonance as seen in Fig. 2(a) reaching the value of 2800 near 2 eV.

Our goal is to take plasmonic effects (i.e., local-field enhancement and phase accumulation) directly into account and investigate how such crafted local fields affect transport properties of molecular junctions placed in the gap of bowtie antennas. However, it is informative first to examine general features of chirped pulses interacting with plasmonic materials. It has been noted in several papers[35–38] that the local-field enhancement depends sensitively on the sign of chirped excitation pulses. Moreover, careful examination of spatiotemporal dependence of local fields on chirp rates[38] revealed a complex dynamics of plasmon wave packets that are noticeably influenced by chirped laser pulses—one may find different local points for a given plasmonic system where positive chirps lead to higher local fields, and the other way around.

Generally speaking, plasmonic materials can be considered as pulse shapers[39] due to the high material dispersion near plasmon resonances, which induces a phase in the frequency

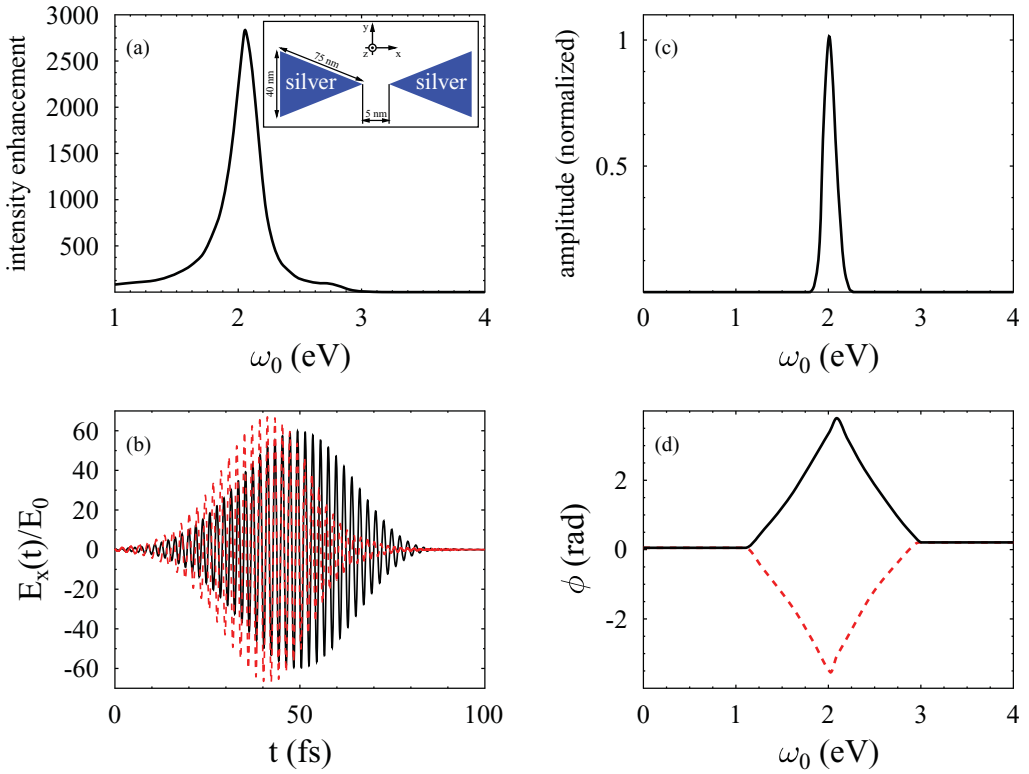

FIG. 2. (Color online) Results of FDTD simulations for chirped pulses exciting the bowtie antenna schematically depicted in the inset of panel (a). Panel (a) shows the enhancement of the local intensity $|\vec{E}|^2$ detected in the gap of the bowtie antenna as a function of the incident frequency. Panel (b) presents a local field component of the electric field along the axis of symmetry of the structure, E_x, as a function of time for two chirp rates at the plasmon resonance, $\omega_0 = 2.057$ eV: black solid line for $\Phi''(\nu_0) = -3000$ fs^2 and red dashed line for $\Phi''(\nu_0) = 3000$ fs^2. Panel (c) shows the amplitude of the local field in the frequency domain (note that it is independent of the phase rate). Panel (d) represents the phase of the local field in the frequency domain at two chirped rates: black solid line for $\Phi''(\nu_0) = -3000$ fs^2 and red dashed line for $\Phi''(\nu_0) = 3000$ fs^2.

domain resulting in a shaping of the total electromagnetic field in the time domain. This is illustrated in Figs. 2(b)–2(d), where one can clearly see that the positive chirp leads to the compression of the local field [Fig. 2(b)] and hence to a stronger field enhancement. While the field amplitude in the frequency domain is not affected by the chirp sign [Fig. 2(c)], obviously the phase of the field is significantly different for positive and negative chirp as shown in Fig. 2(d). We note that one can not recover data obtained for a negative chirp, for instance, by simply flipping the sign of the phase for the positive chirp. The additional phase induced by the plasmonic system, which depends on the sign of the chirp rate, makes this problem time irreversible.[35]

IV. CURRENT THROUGH THE JUNCTION

The time-dependent current through the junction under external driving is[23,40]

$$I_K(t) = -\frac{e}{\hbar}\Big(\mathrm{tr}[\Gamma^K \rho(t)] + \frac{1}{\pi}\mathrm{Im}\int_{-\infty}^{+\infty} dE f_K(E) \times \mathrm{tr}[\Gamma^K \mathbf{G}^r(t,E)]\Big). \quad (8)$$

Here, the trace is taken over the molecular subspace, Γ^K is the matrix of electronic decoherence due to coupling to a contact K

$$\Gamma^K_{mm'} \equiv 2\pi \sum_{k\in K} V_{mk}\, V_{km'}\, \delta(E-\varepsilon_k), \quad (9)$$

which is energy independent in the wide-band approximation, $f_K(E)$ is the Fermi-Dirac thermal distribution in the contacts, $\rho(t) \equiv -i\mathbf{G}^<(t,t)$ is the nonequilibrium-reduced density matrix of molecular subsystem, $\mathbf{G}^{r,<}(t,t')$ are matrices of retarded and lesser projections of the single-electron Green function in the molecular subspace,

$$G_{mm'}(\tau,\tau') \equiv -i\langle T_c\, \hat{d}_m(\tau)\, \hat{d}^\dagger_{m'}(\tau')\rangle, \quad (10)$$

where T_c is a contour-ordering operator, and $\mathbf{G}^r(t,E)$ is the right-side Fourier transform of the retarded Green function,

$$\mathbf{G}^r(t,E) = \int_{-\infty}^{+\infty} dt'\, e^{iE(t-t')}\, \mathbf{G}^r(t,t'). \quad (11)$$

We are interested mostly in the effectiveness of the device as a charge pump, i.e., we will calculate the *excess charge* transferred through the system during the laser pulse,

$$Q_K(t) = \int_{-\infty}^{t} dt' \left[I_K(t') - I_K^{\mathrm{dc}}\right], \quad (12)$$

where $I_K(t)$ is defined in Eq. (8) and $I_K^{\rm dc}$ is the current at bias-induced steady-state conditions, i.e., in the absence of radiation, $E(t) = 0$.

V. EQUATIONS OF MOTION

Markov approximation, employed in Ref. 29, comes from a consideration of time-local quantities only. This approach is sufficient when one can neglect the broadening of molecular states induced by hybridization with states in the contacts. In realistic molecular junctions such a hybridization is non-negligible, since molecules are usually chemisorbed on at least one of the contacts. Here, in addition to the local field formation, we are going to explore how non-Markovian effects influence the characteristics of laser-pulse-induced charge pumping.

To keep non-Markov effects we use the single-particle Green function of Eq. (10) (a time-nonlocal quantity) in our considerations. We employ a Keldysh-contour-based EOM approach, similar to the one employed in our earlier publication[41] (see Appendix A for a derivation):

$$\begin{aligned} i\frac{\partial}{\partial\tau}G_{mm'}(\tau,\tau') &= \delta_{m,m'}\delta(\tau,\tau') + \varepsilon_m G_{mm'}(\tau,\tau') - \mu E(t) G_{\bar{m}m'}(\tau,\tau') \\ &+ \sum_{m_1}\int_c d\tau_1 \Sigma_{mm_1}(\tau,\tau_1) G_{m_1m'}(\tau_1,\tau') - i\sum_{k_1\neq k_2}\sum_{m_1}\left|V^{\rm en}_{k_1k_2}\right|^2 \\ &\times \int_c d\tau_1 g_{k_2}(\tau,\tau_1) g_{k_1}(\tau_1,\tau)\mathcal{G}_{\bar{m}\bar{m}_1,m'm_1}(\tau,\tau_1;\tau',\tau_1+). \end{aligned} \tag{13}$$

Here, $\bar{m}$ is a molecular level other than m (e.g., for $m = 1$, $\bar{m} = 2$), $g_k(\tau,\tau')$ is the single-particle Green function of free electrons in the contacts

$$g_k(\tau,\tau') \equiv -i\langle T_c\, \hat{c}_k(\tau)\,\hat{c}_k^\dagger(\tau')\rangle. \tag{14}$$

$\Sigma_{mm'}(\tau,\tau') \equiv \sum_{K=L,R}\Sigma^K_{mm'}(\tau,\tau')$ is the self-energy due to coupling to contacts with

$$\Sigma^K_{mm'}(\tau,\tau') \equiv \sum_{k\in K} V_{mk} g_k(\tau,\tau') V_{km'} \tag{15}$$

and $\mathcal{G}$ is the molecular-subspace two-particle Green function (GF)

$$\begin{aligned} &\mathcal{G}_{m_1m_2,m_3m_4}(\tau_1,\tau_2;\tau_3,\tau_4) \\ &\equiv -\left\langle T_c\,\hat{d}_{m_1}(\tau_1)\,\hat{d}_{m_2}(\tau_2)\,\hat{d}^\dagger_{m_4}(\tau_4)\hat{d}^\dagger_{m_3}(\tau_3)\right\rangle. \end{aligned} \tag{16}$$

Note that when deriving Eq. (13), we treated the energy-transfer term, given by Eq. (3), in the second-order perturbation theory. Non-Markov effects are preserved in this derivation.

The presence of many-body interactions does not allow us to close the hierarchy (which, in general, is infinite) of equations exactly. To make the problem tractable, we employ the Markov approximation in treating energy transfer, the last term on the right in Eq. (13), and in writing EOM for the two-particle GF (see below). The physics of this approximation comes from the assumption that all the excitons have the same energy, $\Delta\varepsilon = \varepsilon_2 - \varepsilon_1$, which is justified when $\Delta\varepsilon \gg \Gamma_{mm}$ ($m = 1,2$). The latter is a reasonable approximation for the parameters used in our calculations. These approximations are similar to those introduced previously in Refs. 20 and 29.

The molecule-contact coupling in Eq. (13) is treated exactly thus introducing non-Markov effects into the description. This leads to a system of equations (see Appendix A for a derivation):

$$\begin{aligned} i\frac{\partial}{\partial t}G^r_{mm'}(t,E) &= \delta_{m,m'} + (\varepsilon_m - E)G^r_{mm'}(t,E) - \mu E(t) G^r_{\bar{m}m'}(t,E) \\ &- \frac{i}{2}\sum_{m_1=1,2}\Gamma_{mm_1}G^r_{m_1m'}(t,E) \end{aligned} \tag{17}$$

$$\begin{aligned} \frac{d}{dt}n_m(t) &= 2(-1)^m \mu E(t)\mathrm{Im}[p(t)] - \Gamma_{mm}n_m(t) - \Gamma_{m\bar{m}}\mathrm{Re}[p(t)] \\ &+ 2\mathrm{Re}\sum_{m_1}\int_{-\infty}^{+\infty}\frac{dE}{2\pi}G^r_{mm_1}(t,E)\Sigma^<_{m_1m}(E) \\ &- (-1)^m\left(B(\varepsilon_{21})N_M(t) - B(\varepsilon_{12})[n_1(t) - n_2(t) + N_M(t)]\right) \end{aligned} \tag{18}$$

$$\begin{aligned} \frac{d}{dt}p(t) &= -i\mu E(t)(n_2(t) - n_1(t)) - i(\varepsilon_2 + \varepsilon_1)p(t) \\ &- \frac{\Gamma_{21}}{2}(n_1(t) + n_2(t)) - \frac{\Gamma_{11} + \Gamma_{22}}{2}p(t) \\ &+ \sum_{m_1=1,2}\int_{-\infty}^{+\infty}\frac{dE}{2\pi}\left(G^r_{2m_1}(t,E)\Sigma^<_{m_11}(E)\right. \\ &\left. - \Sigma^<_{2m_1}(E)\overset{*}{G}{}^r_{1m_1}(t,E)\right) - i\sum_{m_1}B(\varepsilon_{m_1\bar{m}_1})\mathrm{Im}[p(t),] \end{aligned} \tag{19}$$

$$\begin{aligned} \frac{d}{dt}N_M(t) &= 2\mu E(t)\mathrm{Im}[p(t)] - i\Sigma^<_{22}(\varepsilon_2)n_1(t) \\ &+ i\Sigma^>_{11}(\varepsilon_1)n_2(t) - 2i]\Sigma^>_{12}(\varepsilon_1) + \Sigma^<_{12}(\varepsilon_2)]\mathrm{Re}[p(t)] \\ &- [\Gamma_{11} + \Gamma_{22} + B(\varepsilon_{21})]N_M(t) \\ &+ B(\varepsilon_{12})[n_1(t) - n_2(t) + N_M(t)] \end{aligned} \tag{20}$$

Here, $\varepsilon_{m\bar{m}} \equiv \varepsilon_m - \varepsilon_{\bar{m}}$, $n_m(t) \equiv \rho_{mm}(t)$ ($m = 1,2$) are populations of molecular levels, $p(t) \equiv \rho_{21}(t)$ is molecular coherence, $N_M(t) \equiv \langle\hat{D}^\dagger(t)\hat{D}(t)\rangle \equiv \mathcal{G}_{12,12}(t+,t;t,t+)$ is the molecular excitation correlation function, $\Gamma_{mm'} \equiv \sum_{K=L,R}\Gamma^K_{mm'}$ is the matrix of electronic decoherence due to electron transfer between the molecule and the contacts, with $\Gamma^K_{mm'}$ defined in Eq. (9), $\Sigma^{>,<}_{mm'}(E) = \sum_{K=L,R}\Sigma^{K>,<}_{mm'}(E)$ greater (lesser) projections of self-energy due to coupling to contacts with

$$\Sigma^{K<}_{mm'}(E) \equiv i\Gamma^K_{mm'}f_K(E), \tag{21}$$

$$\Sigma^{K>}_{mm'}(E) \equiv -i\Gamma^K_{mm'}[1 - f_K(E)], \tag{22}$$

and $B(E)$ is the dissipation rate due to energy transfer,

$$\begin{aligned} B(E) \equiv 2\pi\sum_{K=L,R}\sum_{k_1\neq k_2\in K}\left|V^{\rm en}_{k_1k_2}\right|^2\delta\left(\varepsilon_{k_1} - \varepsilon_{k_2} + E\right) \\ \times f_K\left(\varepsilon_{k_1}\right)\left[1 - f_K\left(\varepsilon_{k_2}\right)\right]. \end{aligned} \tag{23}$$

Note that in Eq. (17) we omitted the term coming from energy transfer, since the contribution to the total retarded self-energy, Σ^r, from the molecule-contacts electron transfer, which is $\sim\Gamma$, is much bigger than the corresponding contribution from energy transfer, which is $\sim B(\varepsilon_{21})n_2$ [$\sim B(\varepsilon_{21})(1-n_1)$] for $m=1$ ($m=2$) in a reasonable parameter range.[16,20] The equations of motion [Eqs. (17)–(20)] form a closed set of time-dependent equations to be solved simultaneously on an energy grid starting from a steady-state initial condition corresponding to a biased junction before the laser is switched on. The density matrix, $\rho(t)$, and retarded GF, $\mathbf{G}^r(t,E)$, obtained as a solution, are used in Eqs. (8) and (12) to calculate the time-dependent current and excess charge pumped through the junction, respectively.

In the limit of weak molecule-contact coupling, $\Gamma\to 0$, neglecting local-field and non-Markov effects, disregarding off-diagonal terms in the spectral function, and assuming rotating-wave approximation, reduces Eqs. (17)–(20) to the results of Ref. 29 (see Appendix B for details).

VI. RESULTS AND DISCUSSION

Here, we present results of numerical simulations for a model, see Eqs. (1)–(3), with local-field formation and non-Markov effects taken into account as described above. The time-dependent local electromagnetic field is calculated by solving the Maxwell's equations on a grid (see Sec. III) for metallic contacts of a bowtie geometry. The molecule is placed in a "hot spot" situated between the contacts and a local field plays the role of an external driving force in the electronic calculations (as described in Sec. V).

The parameters of our calculations are chosen to represent a usual molecular-junction situation. Their values are estimated from experimental data as discussed in our previous publication.[23] Unless stated otherwise, the parameters of the electronic simulations are the following: the temperature is 300 K, the molecular electronic-level positions are $\varepsilon_1=-1$ eV and $\varepsilon_2=1$ eV, the elements of the electronic-decoherence matrix are $\Gamma^L_{11}=\Gamma^R_{22}=0.1$ eV, $\Gamma^L_{22}=\Gamma^R_{11}=0.01$ eV, $\Gamma^{L,R}_{12}=\Gamma^{L,R}_{21}=0$, and the coupling to the external field is $\mu\mathcal{E}_0=0.008$ eV (after normalization of Eq. (7) for $\Phi''=2000$ fs^2; also below, the coupling to the external field is given renormalized according to Eq. (7) for a particular Φ''). The Fermi energy is taken as the origin, $E_F=0$, and the bias is applied symmetrically: $\mu_{L,R}=E_F\pm|e|V_{\rm sd}/2$. All calculations below, except those presented in Fig. 6, are done at equilibrium, $V_{\rm sd}=0$. Only the processes of energy relaxation on the molecule are taken into account with $B(\varepsilon_{12})=0$ and $B(\varepsilon_{21})=0.1$ eV. The time grid is taken from the external-driving-field simulations. The energy grid spans a region from -20 to 20 eV with a 0.001 eV step. Other parameters are introduced separately for each calculation.

Figure 3 demonstrates pumped-charge buildup during the laser-pulse excitation. One sees that the local-field formation leads to asymmetry in pumped charge for opposite chirp rates. A negatively chirped incoming field creates a longer local pulse [see Fig. 2(b)], which results in an increase in the total charge pumped through the junction. The role of electron-hole excitations in the contacts on the charge buildup is shown in Fig. 3(a). Since the processes of escaping from

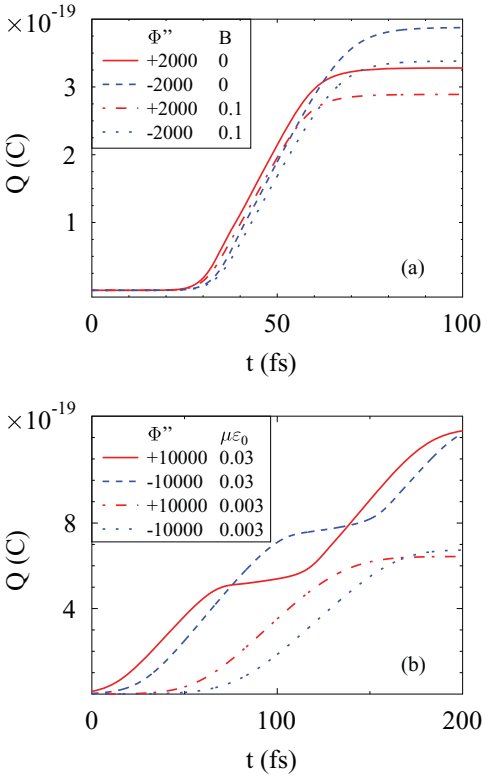

FIG. 3. (Color online) Time dependence of charge pumped through the junction, Q(t), see Eq. (12) for several chirp rates. Shown are results for (a) $\Phi''=2000$ and -2000 fs^2 without energy transfer, $B(\varepsilon_{21})=0$ (red solid line and blue dashed line, respectively), and taking into account energy transfer term, $B(\varepsilon_{21})=0.1$ eV (red dash-dotted line and blue dotted line, respectively) and (b) $\Phi''=10\,000$ and $-10\,000$ fs^2 for $B(\varepsilon_{21})=0.1$ eV and $\mu\mathcal{E}_0=0.03$ (red solid line and blue dashed line, respectively) and $\mu\mathcal{E}_0=0.003$ eV (red dash-dotted line and blue dotted line, respectively).

LUMO into the right contact and energy relaxation on the molecule compete for the excited-state population, the current (and, consequently, the pumped charge) decreases with an increase of coupling to the electron-hole excitations in the contacts. Figure 3(b) shows the effect of intensity of the incoming pulse on the transferred charge buildup. For higher intensity, the buildup demonstrates a saturation in the middle of the pulse. The reason for this behavior is the competition between timescales related to Rabi oscillations induced by the local field between molecular levels and the electronic escape rate from the molecule into the contacts (which is $\sim 1/\Gamma$). On one hand, both negatively and positively chirped pulses in the middle have a frequency approximately at the resonance with the HOMO-LUMO transition, $\omega\approx\varepsilon_2-\varepsilon_1$, which is a prerequisite for effective electron transfer and thus an increase in pumped charge. On the other hand, at resonance Rabi oscillations[42] at high enough intensities compete with the electron escape rate, thus effectively blocking current through the junction. Depending on parameters, this may lead either to the most effective charge transfer in the middle of the pulse [dash-dotted and dotted lines in Fig. 3(b)] or to a suppression of charge transfer at this point [solid and dashed lines in Fig. 3(b)]. Note that the effect is not related to a non-Markov relaxation, i.e., this behavior is observed

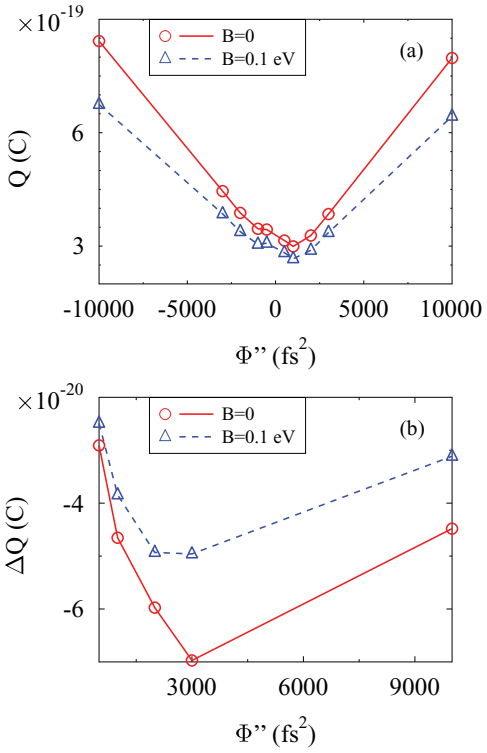

FIG. 4. (Color online) Charge pumped through the junction during a pulse vs. chirp rate: (a) total charge, i.e., the integral of Q(t), see Eq. (12), over the local-field-pulse duration and (b) asymmetry in charge transfer between positively and negatively chirped incoming laser pulses, $\Delta Q \equiv Q(|\Phi''|) - Q(-|\Phi''|)$. Shown are results with $B(\varepsilon_{21}) = 0.1$ eV, blue dashed line with triangles, and without energy transfer, $B(\varepsilon_{21}) = 0$, red solid line with circles.

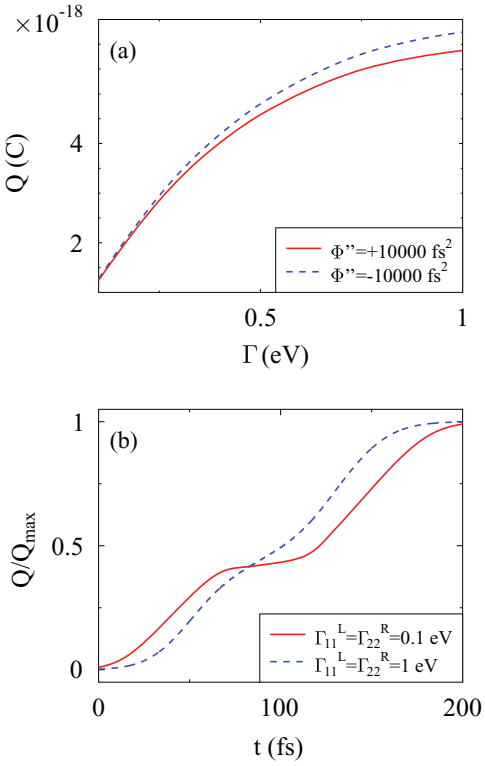

FIG. 5. (Color online) Dependence of charge pumping on the molecule-contact states hybridization at $\mu\mathcal{E}_0 = 0.03$ eV. Shown are (a) charge pumped through the junction during a pulse vs. electronic escape rate for chirp rate $\Phi'' = 10\,000$ fs^2 (red solid line) and $-10\,000$ fs^2 (blue dashed line) and (b) normalized transferred charge buildup (i.e., charge normalized to the total charge transferred during a pulse) vs. time for chirp rate $\Phi'' = 10\,000$ fs^2 and $\Gamma_{11}^L = \Gamma_{22}^R = 0.1$ eV (red solid line) and 1 eV (blue dashed line). The red line in panel (b) is the same as the solid red line in Fig. 3(b).

also in the absence of hybridization between the molecule and the contact(s) states and its relation to the Landau-Zener problem,[43] in terms of total charge pumped across the junction, was discussed in Ref. 29. Note also, that with positively chirped pulse changing frequency from lower to higher values, the transferred-charge buildup is more effective at the start of the pulse (at lower frequencies), while for negatively chirped pulse, a more effective buildup takes place at the end of the pulse [compare solid and dashed lines in Figs. 3(b) and 5(b)]. Contrary to the buildup suppression in the middle of the pulse, this effect is due to the molecule-contact hybridization. The latter leads to a broadening of molecular levels and the effectiveness of HOMO-LUMO charge transfer depends (among other conditions) on the integral of occupied states at the HOMO and empty states at the LUMO separated by the frequency of incident light, $\int dE G_{11}^{<}(E) G_{22}^{>}(E+\omega)$. Clearly, at frequencies below the resonance the latter is greater than at frequencies above it.

The local-field asymmetry relative to the sign of the chirp rate in the frequency domain leads to asymmetry in charge pumping contrary to the symmetric situation presented in Ref. 29, as demonstrated in Fig. 4(a). One can see that the pumped charge is almost symmetric at high rates with an asymmetry confined to the low-rate region. The difference between the charge pumped through the junction at positive and negative chirp rates is shown in Fig. 4(b). As discussed above, the duration of the local field due to positively chirped incoming pulse is shorter than the one due to negatively chirped analog. This compression is the cause of less charge being pumped through the system in the former case, which results in a decrease in $\Delta Q \equiv Q(\Phi'') - Q(-\Phi'')$ in the region of $\Phi''(\nu_0)$ from 0 to 3000 fs^2. Indeed, at the very low-rate frequency the pulse does not change much, so the asymmetry is solely due to the difference in the pulse length. At the higher rates an additional factor appears; the most effective contribution to charge transfer takes place at a particular region of frequencies (at and just below the resonance, as is discussed above). This region is passed faster in the positively chirped local pulse, and in the region up to 3000 fs^2 this results in an increase of asymmetry, since negatively chirped pulse spends more time in its effective-frequencies zone. Further increase of chirp rate leads to decrease and almost disappearance of the asymmetry. The reason is the decrease of ratio of the pulses difference to the overall local-pulse duration.

The coupling to electron-hole excitations not only diminishes the pumped charge [compare solid and dashed lines in Fig. 4(a)], but also decreases the asymmetry [see Fig. 4(b)]. The latter results from the fact that the rate for molecular energy relaxation (LUMO $\rightarrow$ HOMO transition due to coupling to excitations in the contacts) is proportional

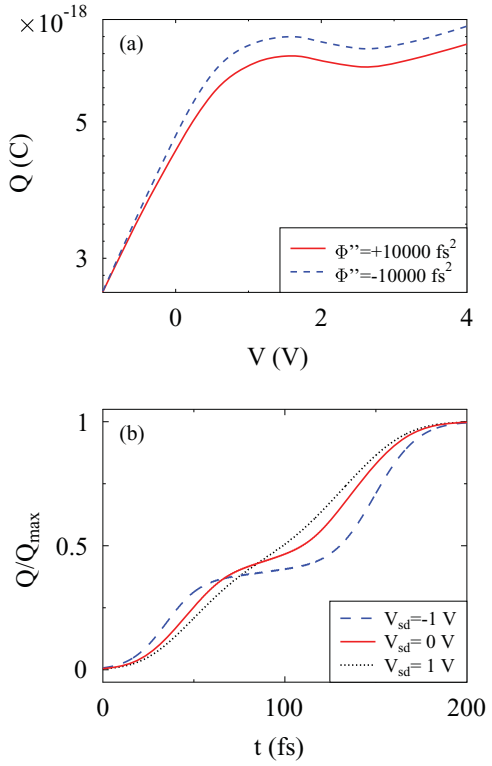

FIG. 6. (Color online) Dependence of charge pumping on bias. (a) Total excess charge pumped through the junction during a pulse vs. bias for chirp rate $\Phi'' = 10\,000$ fs^2 (red solid line) and $-10\,000$ fs^2 (blue dashed line). (b) Excess charge buildup (normalized to the total excess charge transferred during a pulse) vs. time at chirp rate $\Phi'' = 10\,000$ fs^2 for $V_{sd} = -1$ V (blue dashed line), 0 V (red solid line), and 1 V (black dotted line). Here, $\Gamma^L_{11} = \Gamma^R_{22} = 0.5$ eV. The red line in panel (b) is the same as the solid red line in Fig. 3(b).

to the population in the LUMO (see discussion in Ref. 20). So for higher currents, the energy relaxation also will be more efficient, thus effectively compensating for the difference.

The importance of non-Markov behavior for a charge pump is demonstrated in Fig. 5. Figure 5(a) shows pumped charge as a function of the level width (for two opposite choices of chirp rate). The increase in the total charge pumped through the junction with the increase in hybridization saturates at high strengths of coupling between the molecule and the contacts. Such behavior is expected; at low hybridization there is only one frequency corresponding to a resonance, where pumping is most effective, so only an "instant" of chirped pulse contributes to the charge transfer. As the molecule-contact coupling grows the condition of resonance transition becomes less and less strict. Eventually, any frequency within the chirped pulse has roughly the same effectiveness—this is the reason for the saturation. Also, stronger coupling means more effective molecule-contact electron transfer, which competes more effectively with the intramolecular Rabi oscillations at the resonance. This competition is demonstrated in Fig. 5(b), where the middle-of-the-pulse saturation (see discussion of Fig. 3) disappears for stronger molecule-contact couplings.

Finally, in Fig. 6 we discuss the influence of bias on charge pumping. Here, we define the optically pumped charge (or excess charge) as a difference between charge pumped through the junction with and without a laser field. Figure 6(a) demonstrates total excess-pumped charge during a laser pulse for opposite choices of chirp rate as a function of bias. The application of bias has two effects on the pumping process: (1) it depletes (populates) the HOMO (the LUMO) and (2) it may block or release channels for electron transfer from LUMO to contact R. This leads to a situation when the most effective optical pumping does not correspond to the zero bias, rather we see a shallow peak at $V \sim 1$ V. The explanation is related to the fact that the broadened molecular levels are, essentially, a set of scattering channels with different transmission probabilities; high-conducting channels are in the center of the Lorentzian, while channels on the sides of the distribution are poor conductors. An optical process takes an electron from an occupied ground state and puts it in one empty excited state. The effectiveness of the charge pump is defined by the increase or decrease of current through the junction under an optical pulse (see discussion in Ref. 23). In particular, negative bias decreases the effectiveness of the pump mostly due to blocking part of LUMO-R escape routes. Positive bias opens additional escape routes at the tail of LUMO Lorentzian facilitating increase in pump efficiency. However, an additional effect of depleting HOMO and populating LUMO partially blocks optically induced HOMO-LUMO electron transfer thus reducing overall the effectiveness of optical pumping. The competition between the two processes reveals itself as a shallow peak at $\sim$1 V.

The time-resolved charge buildup is presented in Fig. 6(b). The middle-of-the-pulse saturation observed previously at the equilibrium [solid line, same as in Fig. 3(b)] is enhanced at negative (dashed line) and disappears at positive bias (dotted line). The reason is similar to the competition between the Rabi frequency and the escape rate discussed above. Indeed, with negative bias partially blocking fast escape route for the electron from an excited state into the right contact, Rabi oscillations play an important role at the quasiresonant situation in the middle of the pulse. Positive bias, by opening additional routes, makes the Rabi oscillations less effective.

VII. CONCLUSIONS

We consider a two-level (HOMO-LUMO) model for an optically-driven molecular charge pump. Such a pump may be realized as a junction formed by a molecule with strong charge-transfer transitions between its ground and excited states. The junction is driven by both an applied bias and a laser pulse. The latter is treated as a classical external driving force.

Our consideration is a generalization of the previous study,[29] which takes into account effects of local field ("hot-spot" formation) and hybridization between the states of the molecule and the contact(s) (i.e., non-Markov effects). We formulate an approximate closed set of equations of motion for single- and two-particle GFs. The electron transfer in the former is treated exactly. To close the set of equations, the latter is considered within the Markov approximation. Our equations of motion are reduced to the set of equations derived in Ref. 29, under several simplifying assumptions: weak molecule-contact coupling (i.e., neglect of hybridization), neglect of the nondiagonal terms in the molecular spectral

function, and an equations-of-motion set within the rotating-wave approximation.

The incoming laser pulse is assumed to be linearly chirped. The local field is calculated within FDTD technique on a grid with a bowtie antenna geometry used to represent junction metallic contacts. We find that contrary to the symmetric behavior of the pump relative to the sign of the chirp rate, as reported previously,[29] the duration of the corresponding local-field pulse depends on the sign of incoming chirp, which results in an asymmetric operation of the pump. The asymmetry depends on the incoming pulse chirp rate in a nonmonotonic manner. We find that the junction response to optical driving is symmetric to both low and high chirp rates going through a maximum between the two extremes. This behavior is caused by the correspondence between the pulse duration of the local field and the detuning of its frequency at the end of the pulse from the energy difference between the molecular states, $(\varepsilon_2 - \varepsilon_1)$.

We note that at a quasiresonance the charge pump becomes ineffective due to the competition between intramolecular Rabi oscillations induced by a pulse with electron transfer from the molecule to the contact. Increase of the molecule-contact-coupling strength increases the electron escape rate thus reducing the ineffectiveness of the pump due to Rabi oscillations. This indicates a necessity of taking into account the broadening of molecular states, which requires a treatment beyond the Markov approximation of Ref. 29. The most effective charge-pump regime is found at finite positive bias rather than at the equilibrium as one might have expected from the Markov consideration of Ref. 29. The effect comes from optically assisted charge redistribution between low- and high-conducting scattering channels in broadened molecular states (see our previous publication[23] for a detailed discussion). Within the model, negative bias reduces (and positive increases) excess-charge pumping due to blocking (facilitating) outgoing scattering channels in the excited molecular state and thus increasing (decreasing) the role of intramolecular Rabi oscillations.

Finally, we note that the direct electron-hole excitation in the contacts, heating, and inelastic effects are examples of effects beyond the current consideration, which may also have a significant impact on the properties of a molecular charge pump.

ACKNOWLEDGMENTS

We acknowledge support by the National Science Foundation (MG, CHE-1057930), the US-Israel Binational Science Foundation (BF and MG, No. 2008282), and the UCSD (MG, startup funds).

APPENDIX A : DERIVATION OF EQ. (13)

EOM for Eq. (13) in a contour variable, τ, starts from writing the Heisenberg equation for $\hat{d}_m(\tau)$

$$i\frac{\partial}{\partial\tau}G_{mm'}(\tau,\tau') = \delta_{m,m'}\delta(\tau,\tau') + \varepsilon_m G_{mm'}(\tau,\tau') - \mu E(t)G_{\bar{m}m'}(\tau,\tau') + \sum_k V_{mk}G_{km'}(\tau,\tau') + \sum_{k_1\neq k_2} V^{\rm en}_{k_1k_2}\mathcal{G}_{\bar{m}k_2,m'k_1}(\tau-,\tau;\tau',\tau+) \quad \text{(A1)}$$

Here, $\tau+$ $(\tau-)$ indicates a variable immediately after (before) τ on the contour. The last two terms on the right come from the electron- and energy-transfer terms in Eq. (3). Treating the two within the noncrossing approximation allows us to find the first exactly within a standard procedure,[44]

$$G_{km'}(\tau,\tau') = \sum_{m_1}\int_c d\tau_1 g_k(\tau,\tau_1)V_{km_1}G_{m_1m'}(\tau_1,\tau'). \quad \text{(A2)}$$

The two-particle Green function in the second term is treated (still keeping noncrossing approximation in mind) within the first-order perturbation theory in energy transfer,

$$\mathcal{G}_{\bar{m}k_2,m'k_1}(\tau,\tau;\tau',\tau) = -iV^{\rm en}_{k_2k_1}\sum_{m_1}\int_c d\tau_1 g_{k_2}(\tau,\tau_1)g_{k_1}(\tau_1,\tau) \times \mathcal{G}_{\bar{m}\bar{m}_1,m'm_1}(\tau,\tau_1;\tau',\tau_1+) \quad \text{(A3)}$$

Substituting (A2) and (A3) into (A1) yields Eq. (13).

Equation (17) is the retarded projection of Eq. (13) with omitted energy transfer term. The approximation is based on an estimate that, in a usual situation, the electron escape rate should be much bigger than the corresponding energy transfer.[16]

Equations (18) and (19) are lesser projections of Eq. (13) taken at equal times, $-i\mathbf{G}^<(t,t)$. Note that Eq. (19) is exact, while in Eq. (18) we employ the Markov approximation for the derivation of the energy-transfer term, similar to previous publications,[20,29] for example,

$$\begin{aligned}\sum_{k_1\neq k_2}\sum_{m_1}\int_{-\infty}^{t} dt_1 g^>_{k_2}(t-t_1)g^<_{k_1}(t_1-t)\left\langle\hat{d}^\dagger_m(t)\hat{d}_{\bar{m}}(t)\hat{d}^\dagger_{m_1}(t_1)\hat{d}_{\bar{m}_1}(t_1)\right\rangle \\ \approx \int_{-\infty}^{t} dt_1 g^>_{k_2}(t-t_1)g^<_{k_1}(t_1-t)e^{i(\varepsilon_{m_1}-\varepsilon_{\bar{m}_1})(t_1-t)} \\ \times\left\langle\hat{d}^\dagger_m(t)\hat{d}_{\bar{m}}(t)\hat{d}^\dagger_{m_1}(t)\hat{d}_{\bar{m}_1}(t)\right\rangle \\ \approx \left[1-n_{k_2}\right]n_{k_1}\pi\delta\left(\varepsilon_{k_2}-\varepsilon_{k_1}+\varepsilon_{m_1}-\varepsilon_{\bar{m}_1}\right) \\ \times\left\langle\hat{d}^\dagger_m(t)\hat{d}_{\bar{m}}(t)\hat{d}^\dagger_{m_1}(t)\hat{d}_{\bar{m}_1}(t)\right\rangle. \end{aligned} \quad \text{(A4)}$$

Using Eq. (A4) and similar expressions for other parts of the Keldysh contour, which is deformed in accordance with Langreth rules,[44] in the energy-transfer term of a lesser projection of the diagonal element of Eq. (13), and utilizing Eq. (23), leads to Eq. (18).

Finally, Eq. (20) is treated with the Markov approximation [see Eq. (A4) above] applied to both electron- and energy-transfer terms. Then the derivation goes along the lines presented in Ref. 29.

APPENDIX B : MARKOV LIMIT OF EQS. (17)– (20)

The equations of motion derived in Ref. 29 are the Markov limit of Eqs. (18)– (20) within a static quasiparticle approximation assumed for the molecular states. The latter implies disregarding Eq. (17) and assuming instead

$$i\left[G^r_{mm'}(t,E) - G^a_{mm'}(t,E)\right] = 2\pi\delta_{m,m'}\delta(E-\varepsilon_m). \quad \text{(B1)}$$

Then, disregarding the level mixing due to coupling to contacts, $\Gamma^K_{12} = \Gamma^K_{21} = 0$, Eqs. (18) and (19) are reduced to the Eqs. (33) and (34)[45] of Ref. 29. After omitting the nondiagonal elements of self-energy in Eq. (20) one gets Eq. (35) of Ref. 29.

[1] P. Hänggi, Nat. Mater.**10**, 6 (2011).
[2] E. M. Roeling, W. C. Germs, B. Smalbrugge, E. J. Geluk, T. de Vries, R. A. J. Janssen, and M. Kemerink, Nat. Mater. **10**, 51 (2011).
[3] V. Siegle, C.-W. Liang, B. Kaestner, H. W. Schumacher, F. Jessen, D. Koelle, R. Kleiner, and S. Roth, Nano Lett. **10**, 3841 (2010).
[4] R. Hanson, L. P. Kouwenhoven, J. R. Petta, S. Tarucha, and L. M. K. Vandersypen, Rev. Mod. Phys. **79**, 1217 (2007).
[5] L. Bogani and W. Wernsdorfer, Nat. Mater. **7**, 179 (2008).
[6] A. Nitzan, Science **317**, 759 (2007).
[7] Z. Wang, J. A. Carter, A. Lagutchev, Y. K. Koh, N.-H. Seong, D. G. Cahill, and D. D. Dlott, Science **317**, 787 (2007).
[8] N. J. Halas, Nano Lett. **10**, 3816 (2010).
[9] R. Hildner, D. Brinks, and N. F. van Hulst, Nature Phys. **7**, 172 (2011).
[10] R. J. Gordon, L. Zhu, and T. Seideman, Acc. Chem. Res. **32**, 1007 (1999).
[11] D. R. Ward, N. K. Grady, C. S. Levin, N. J. Halas, Y. Wu, P. Nordlander, and D. Natelson, Nano Lett. **7**, 1396 (2007).
[12] D. R. Ward, N. J. Halas, J. W. Ciszek, J. M. Tour, Y. Wu, P. Nordlander, and D. Natelson, Nano Lett. **8**, 919 (2008).
[13] Z. Ioffe, T. Shamai, A. Ophir, G. Noy, I. Yutsis, K. Kfir, O. Cheshnovsky, and Y. Selzer, Nature Nanotech. **3**, 727 (2008).
[14] D. R. Ward, D. A. Corley, J. M. Tour, and D. Natelson, Nature Nanotech. **6**, 33 (2011).
[15] S. Kohler, S. Camalet, M. Strass, J. Lehmann, G.-L. Ingold, and P. Hänggi, Chem. Phys. **296**, 243 (2004).
[16] M. Galperin, A. Nitzan, and M. A. Ratner, Phys. Rev. Lett. **96**, 166803 (2006).
[17] J. K. Viljas, F. Pauly, and J. C. Cuevas, Phys. Rev. B **76**, 033403 (2007).
[18] J. K. Viljas, F. Pauly, and J. C. Cuevas, Phys. Rev. B **77**, 155119 (2008).
[19] M. Galperin and A. Nitzan, Phys. Rev. Lett. **95**, 206802 (2005).
[20] M. Galperin and A. Nitzan, J. Chem. Phys. **124**, 234709 (2006).
[21] U. Harbola, J. B. Maddox, and S. Mukamel, Phys. Rev. B **73**, 075211 (2006).
[22] M. Galperin and S. Tretiak, J. Chem. Phys. **128**, 124705 (2008).
[23] M. Sukharev and M. Galperin, Phys. Rev. B **81**, 165307 (2010).
[24] M. Galperin, M. A. Ratner, and A. Nitzan, Nano Lett. **9**, 758 (2009).
[25] M. Galperin, M. A. Ratner, and A. Nitzan, J. Chem. Phys. **130**, 144109 (2009).
[26] M. Ponder and R. Mathies, J. Phys. Chem. **87**, 5090 (1983).
[27] V. L. Colvin and A. P. Alivisatos, J. Chem. Phys. **97**, 730 (1992).
[28] S. N. Smirnov and C. L. Braun, Rev. Sci. Instrum. **69**, 2875 (1998).
[29] B. D. Fainberg, M. Jouravlev, and A. Nitzan, Phys. Rev. B **76**, 245329 (2007).
[30] L. Allen and J.-H. Eberly, *Optical Resonance and Two-Level Atoms* (Wiley, New York, London, Sydney, Toronto, 1975).
[31] T. Bryllert, M. Borgstrom, T. Sass, B. Gustafson, L. Landin, L. E. Wernersson, W. Seifert, and L. Samuelson, Appl. Phys. Lett. **80**, 2681 (2002).
[32] R. Sanchez, G. Platero, and T. Brandes, Phys. Rev. B **78**, 125308 (2008).
[33] G. Q. Li, B. D. Fainberg, A. Nitzan, S. Kohler, and P. Hänggi, Phys. Rev. B **81**, 165310 (2010).
[34] A. Taflove and S. C. Hagness, *Computational Electrodynamics: The Finite-Difference Time-Domain Method*, 3rd ed. (Artech House, Boston, 2005).
[35] M. I. Stockman, D. J. Bergman, and T. Kobayashi, Phys. Rev. B **69**, 054202 (2004).
[36] T.-W. Lee and S. K. Gray, Phys. Rev. B **71**, 035423 (2005).
[37] M. Aeschlimann, M. Bauer, D. Bayer, T. Brixner, F. J. Garcia de Abajo, W. Pfeiffer, M. Rohmer, C. Spindler, and F. Steeb, Nature (London) **446**, 301 (2007).
[38] L. Cao, R. A. Nome, J. M. Montgomery, S. K. Gray, and N. F. Scherer, Nano Lett. **10**, 3389 (2010).
[39] A. M. Weiner, *Ultrafast Optics* (Wiley, Hoboken, NJ, 2009).
[40] A. P. Jauho, N. S. Wingreen, and Y. Meir, Phys. Rev. B **50**, 5528 (1994).
[41] M. Galperin, A. Nitzan, and M. A. Ratner, Phys. Rev. B **76**, 035301 (2007).
[42] L. D. Landau and E. M. Lifshitz, *Quantum Mehcanics. Non-relativistic Theory* (Pergamon, Oxford, 1991).
[43] A. Nitzan, *Chemical Dynamics in Condensed Phases* (Oxford University, New York, 2006).
[44] H. Haug and A.-P. Jauho, *Quantum Kinetics in Transport and Optics of Semiconductors* (Springer-Verlag, Berlin, 1996)
[45] Note, Markov limit of Eq. (19) differs from Eq. (34) in Ref. 29, since the latter is written under the additional assumption of the rotating-wave approximation.